Nuclear Mathematical and Computational Sciences: A Century in Review, A Century Anew
Gatlinburg, Tennessee, April 6-11, 2003, on CD-ROM, American Nuclear Society, LaGrange Park, IL (2003)

THE EXPLICIT SLOPE S_N DISCRETIZATION METHOD

Heath L. Hanshaw and Edward W. Larsen
Department of Nuclear Engineering and Radiological Sciences
University of Michigan
Ann Arbor, Michigan USA 48103
hhanshaw@umich.edu, edlarsen@umich.edu

ABSTRACT

The Explicit Slope (ES) discretization method for the S_N transport equation is derived, analyzed, and tested. The ES method preserves linear transport solutions and satisfies the asymptotic thick diffusion limit, while requiring only a single fundamental unknown per cell. We demonstrate the ES method's accuracy compared to other methods having a single unknown per cell. We also show that while a straightforward Diffusion Synthetic Acceleration scheme is not uniformly robust, Krylov solution methods preconditioned with the standard cell-centered diffusion operator are uniformly effective over a wide range of test problems.

Key Words: S_N spatial discretization, diffusion limit, DSA, Krylov methods

1. INTRODUCTION

In the Explicit Slope (ES) S_N discretization [1], in one spatial dimension, the scattering source is assumed to have a piecewise linear-in-space representation. Current methods that treat the scattering source as linear-in-space, such as linear characteristic or linear finite element methods, generally require multiple unknowns per cell or node. Instead of treating the slope of the scattering source as a separate unknown, however, we make an explicit approximation. We express the slopes in terms of a single unknown per cell, the cell-average scalar flux. Fewer unknowns per cell means that (i) storage requirements are reduced, and (ii) preconditioning is simpler because the residual is smaller. Also, the ES method achieves greater accuracy than other schemes with only one unknown per cell, such as Diamond Differencing (DD) and Step Characteristic (SC)[2]. Unlike the SC scheme, the ES method preserves the exact infinite medium linear-in-space solutions of the transport equation [3]. Unlike both the DD and SC schemes, the ES scheme satisfies the thick diffusion limit – it asymptotically limits to a standard cell-centered diffusion discretization with Marshak boundary conditions [4].

In this paper, we present a brief derivation of the basic ES method in planar geometry. We then summarize key elements of the asymptotic analysis. We compare the accuracy of ES to that of DD, SC, and lumped Linear Discontinuous (LD) finite elements on diffusive test problems. The original ES method [1] degrades in unresolved boundary layers at material interfaces due to the diffusive nature of the slope term. We demonstrate this inaccuracy and explain how a simple physically-motivated linear slope limiter can greatly improve accuracy across unresolved boundary layers.

For accelerated iterative solution of the discretized ES equations, we have attempted both additive Diffusion Synthetic Acceleration (DSA) [5] and diffusion preconditioned Krylov [6–8] methods. The asymptotic cell-centered diffusion discretization is effective in DSA for homogeneous-medium problems and for optically thin heterogeneous problems ($\Sigma_t h \sim 1$). Unfortunately, this inconsistent DSA (IDSA)

method becomes unstable for optically thick heterogeneous problems. Application of the consistent four-step approach [5] to the ES scheme results in a complicated, symmetric indefinite 5-point diffusion stencil in 1-D. Neither of these DSA approaches is uniformly cheap and effective. However, Krylov iteration on the scalar flux, preconditioned with the asymptotic cell-centered diffusion discretization, is very effective. We briefly discuss the heterogeneous Fourier analysis of IDSA, then present and discuss Krylov results preconditioned with the cell-centered diffusion operator.

2. DERIVATION

We consider the monoenergetic planar geometry transport equation with isotropic scattering,

$$\left(\mu\frac{\partial}{\partial x}+\Sigma_t(x)\right)\psi(x,\mu)=\frac{1}{2}\left[\Sigma_s(x)\int_{-1}^{1}\psi(x,\mu)\,d\mu+Q(x)\right]. \tag{1}$$

Our essential approach is to discretize the left and right sides of Eq. (1) separately, in as simple a fashion as possible that will guarantee the scheme preserves linear solutions and goes over to a valid, symmetric positive definite discretization of the diffusion equation in the thick asymptotic limit. We discretize on a spatial cell with center x_j and edges $x_{j\pm\frac{1}{2}}$, $j=1:J$, and we use $\mathrm{S_N}$ direction cosines and weights, (μ_n, w_n), $n=1:N$. We assume that material properties are uniform on a spatial cell, integrate Eq. (1) from $x_{j-\frac{1}{2}}$ to $x_{j+\frac{1}{2}}$, and divide by $\Sigma_{tj}h_j=\Sigma_{tj}(x_{j+\frac{1}{2}}-x_{j-\frac{1}{2}})$ to obtain the balance equation

$$\frac{1}{2\tau_{nj}}\left(\psi_{n,j+\frac{1}{2}}-\psi_{n,j-\frac{1}{2}}\right)+\psi_{n,j}=\frac{S_j}{\Sigma_{tj}}, \tag{2}$$

where

$$\tau_{nj} = \frac{\Sigma_{tj}h_j}{2\mu_n}, \tag{3}$$

$$S_j = \frac{1}{2}(\Sigma_{sj}\phi_j+Q_j), \tag{4}$$

$$\phi_j h_j = \int_{x_{j-\frac{1}{2}}}^{x_{j+\frac{1}{2}}}\phi(x)\,dx, \tag{5}$$

$$\phi(x) = \int_{-1}^{1}\psi(x,\mu)\,d\mu, \tag{6}$$

$$Q_j h_j = \int_{x_{j-\frac{1}{2}}}^{x_{j+\frac{1}{2}}}Q(x)\,dx. \tag{7}$$

We generalize the characteristic approach taken in [1] and consider multiple methods of discretizing the left side of the transport equation. Each method leads to a weighted difference auxiliary equation of the form

$$\psi_{n,j}=\frac{1+\alpha_{nj}}{2}\psi_{n,j+\frac{1}{2}}+\frac{1-\alpha_{nj}}{2}\psi_{n,j-\frac{1}{2}}-\frac{\alpha_{nj}}{2\Sigma_{tj}}T_{nj}, \tag{8}$$

where

$$T_{nj}=\frac{1}{2}(\Sigma_{sj}\hat{\phi}_{nj}+\hat{Q}_j). \tag{9}$$

In Eqs. (8) and (9), $\hat{\phi}_{nj}$ and $\hat{Q}_j$ are "slope" terms and the α_{nj} are angle-dependent weights. By construction, we represent the right side of the transport equation (1) as *linear-in-space*,

$$\frac{1}{2}\left[\Sigma_s(x)\int_{-1}^{1}\psi(x,\mu)\,d\mu+Q(x)\right]\approx S_j+T_{nj}\frac{x-x_j}{h_j}. \tag{10}$$

We assume on cell j that

$$Q(x) = Q_j + \hat{Q}_j \frac{x - x_j}{h_j}$$

and

$$\phi(x) = \phi_j + \hat{\phi}_{nj} \frac{x - x_j}{h_j}.$$

For discretization of the left side of the transport equation, we consider two approaches. First, using Eq. (10), we integrate Eq. (1) along characteristics and rearrange (as in [9]) to obtain

$$\alpha_{nj} = \coth(\tau_{nj}) - \frac{1}{\tau_{nj}}. \tag{11}$$

This definition of α_{nj} is identical for both the Step and Linear Characteristic schemes; the difference is that the slope term, T_{nj} in Eq. (8), is set to zero in the Step Characteristic method. Secondly, we consider a linear-in-space discretization of the left side of the transport equation (1). Applying this to Eq. (1) by various means [2, 9, 10], we obtain

$$\alpha_{nj} = \frac{\tau_{nj}}{\theta + |\tau_{nj}|}. \tag{12}$$

Here, $\theta = 1$ corresponds to either a lumped Linear Discontinuous (LD) or to a multiple balance (MB) discretization, and $\theta = 3$ corresponds to regular LD. In this paper, we only consider $\theta = 1$. Once we define an explicit slope approximation, $\hat{\phi}_{nj}$, the two terms, α_{nj} and $\hat{\phi}_{nj}$, completely characterize the 1-D differencing scheme (along with the balance equation (2) and the auxiliary equation (8)).

2.1 Approximation of the Slope Term

To derive the slope term, $\hat{\phi}_{nj}$, we observe that to properly mimic the conservation properties of the first derivative terms in both the transport and diffusion equations, the discrete net current across cell boundaries should be continuous. We wish to achieve this in our approximation of the slope term,$\hat{\phi}_{nj}$, using only the cell-centered scalar fluxes. We begin by writing a discretized slope term for each half-cell in the grid. We then match the half-cell currents on either side of each interface, just as is done in deriving the standard cell-centered diffusion discretization. Specifically, we write a finite-differenced form of the slope term on a half-cell

$$\hat{\phi}_{nj} \approx \begin{cases} \hat{\phi}_{+j} = 2(\tilde{\phi}_{j+\frac{1}{2}} - \phi_j), & \mu_n > 0 \\ \hat{\phi}_{-j} = 2(\phi_j - \tilde{\phi}_{j-\frac{1}{2}}), & \mu_n < 0, \end{cases}$$

where

$$\frac{2(\tilde{\phi}_{j+\frac{1}{2}} - \phi_j)}{3\Sigma_{tj} h_j} = \frac{2(\phi_{j+1} - \tilde{\phi}_{j+\frac{1}{2}})}{3\Sigma_{t,j+1} h_{j+1}}$$

at each interior cell boundary. Letting $t_j = \Sigma_{tj} h_j$ be the normal optical thickness across cell j, we obtain the optical thickness weighted approximate cell-edge fluxes

$$\tilde{\phi}_{j\pm\frac{1}{2}} = \frac{t_j \phi_{j\pm1} + t_{j\pm1} \phi_j}{t_j + t_{j\pm1}}.$$

Using this in our finite-differenced slope term, we obtain $\hat{\phi}_{nj}$ as presented in [1],

$$\hat{\phi}_{n,j} = \hat{\phi}_{\pm,j} = \begin{cases} \frac{2t_j}{t_j + t_{j+1}} \left(\phi_{j+1} - \phi_j\right), & \mu_n > 0, \\ \frac{2t_j}{t_j + t_{j-1}} \left(\phi_j - \phi_{j-1}\right), & \mu_n < 0. \end{cases} \tag{13}$$

This explicitly defines the scattering source slope term in Eq. (9) for interior cells. For exiting directions at boundaries, we define the approximate scalar edge fluxes, $\tilde{\phi}_{\frac{1}{2}}$ and $\tilde{\phi}_{J+\frac{1}{2}}$, exactly as is done in diffusion theory for a Marshak boundary condition. This is consistent with our procedure on interior edges, and it ensures that the asymptotic diffusion equation satisfies the Marshak boundary condition. For example, for a prescribed incident flux on the left boundary $\left(\psi_{n,\frac{1}{2}}, \mu_n > 0\right)$, we set

$$\tilde{\phi}_{\frac{1}{2}} = \frac{4\sum_{\mu_n>0}\mu_n\psi_{n,\frac{1}{2}}w_n + \frac{4}{3t_1}\phi_1}{1+\frac{4}{3t_1}} = \frac{4J_{in}+\frac{4}{3t_1}\phi_1}{1+\frac{4}{3t_1}}$$

to obtain

$$\hat{\phi}_{-,1} = 2(\phi_1 - \tilde{\phi}_{\frac{1}{2}}) = 2\phi_1 - \frac{8J_{in}+\frac{8}{3t_1}\phi_1}{1+\frac{4}{3t_1}}.$$

Thus, in the ES method, the source term [right side of Eq (1)] is represented as a linear function in each spatial cell [Eq. (10)], but the method employs only one fundamental unknown per cell,the cell-average scalar flux [Eq. (13)].

2.2 Thick Diffusion Limit

To examine the behavior of the ES differencing scheme in the asymptotic thick diffusion limit, we make the scaling changes of variables [4]:

$$\begin{aligned}
\Sigma_{tj} &= \epsilon^{-1}\Sigma_{tj}, \\
\Sigma_{sj} &= \epsilon^{-1}\Sigma_{tj} - \epsilon\Sigma_{aj}, \\
Q_j &= \epsilon Q_j, \\
\hat{Q}_j &= \epsilon\hat{Q}_j,
\end{aligned}$$

and let $\epsilon \to 0$. With the characteristic α_{nj} [Eq. (11)], we see that

$$\begin{aligned}
\tau_{nj} &= \epsilon^{-1}\tau_{nj} \\
\alpha_{nj} &= \coth(\epsilon^{-1}\tau_{nj}) - \frac{\epsilon}{\tau_{nj}} \\
&= \frac{\mu_n}{|\mu_n|} - \frac{\epsilon}{\tau_{nj}} + O(e^{-\frac{2\tau_{nj}}{\epsilon}}) \qquad \text{as} \qquad \epsilon \to 0.
\end{aligned} \tag{14}$$

For the linear-in-space α_{nj} [Eq. (12)],

$$\begin{aligned}
\alpha_{nj} &= \frac{\epsilon^{-1}\tau_{nj}}{1+|\epsilon^{-1}\tau_{nj}|} \\
&= \frac{\mu_n}{|\mu_n|} - \frac{\epsilon}{\tau_{nj}} + O(\epsilon^2) \qquad \text{as} \qquad \epsilon \to 0.
\end{aligned} \tag{15}$$

Thus, α_{nj} is the same to $O(\epsilon)$ for both the characteristic and linear discretizations of the left side of the transport equation. Rewriting the balance and auxiliary equations and using the discrete ordinates form of the scalar flux in terms of the angular flux, we obtain asymptotically equivalent balance and auxiliary equations for both approaches:

$$\frac{\epsilon}{2\tau_{nj}}\left(\psi_{n,j+\frac{1}{2}} - \psi_{n,j-\frac{1}{2}}\right) + \psi_{n,j} = \frac{1}{2}\sum_{n=1}^{N}\psi_{n,j}w_n - \epsilon^2\left(\frac{\Sigma_{aj}}{2\Sigma_{tj}}\sum_{n=1}^{N}\psi_{n,j}w_n - \frac{Q_j}{2\Sigma_{tj}}\right), \tag{16}$$

and

$$\psi_{n,j} = \frac{\left(1+\frac{\mu_n}{|\mu_n|}\right)}{2}\psi_{n,j+\frac{1}{2}} + \frac{\left(1-\frac{\mu_n}{|\mu_n|}\right)}{2}\psi_{n,j-\frac{1}{2}} - \frac{1}{4}\frac{\mu_n}{|\mu_n|}\hat{\phi}_{nj} + \epsilon\left(\frac{-2(\psi_{n,j+\frac{1}{2}} - \psi_{n,j-\frac{1}{2}}) + \hat{\phi}_{nj}}{4\tau_{nj}}\right) + O(\epsilon^2). \tag{17}$$

Thus, we are able to perform a common thick diffusion limit analysis. We assume an asymptotic expansion of the angular flux and its discretized values,

$$\psi \sim \sum_{k=0}^{\infty} \epsilon^k \psi^{(k)} \qquad \text{as} \qquad \epsilon \to 0, \tag{18}$$

and we define

$$\phi_j^{(k)} \equiv \sum_{n=1}^{N} \psi_j^{(k)} w_n.$$

We insert the asymptotic expansions into the scaled equations, (16) and (17), and follow the standard limit process. After straightforward algebra, we find that the leading order scalar flux satisfies the standard cell-centered discretization of the diffusion equation

$$-\frac{2}{3(t_j + t_{j+1})}\left(\phi_{j+1}^{(0)} - \phi_j^{(0)}\right) + \frac{2}{3(t_j + t_{j-1})}\left(\phi_j^{(0)} - \phi_{j-1}^{(0)}\right) + \Sigma_{aj}\phi_j^{(0)} h_j = Q_j h_j. \tag{19}$$

In Figures 1 and 2, we compare the thick diffusion accuracy of ES to LD, DD, and SC. In each of Figures 1 through 5, by resolved we mean 10,000 spatial meshes with fixed angular quadrature. Figure 1 describes a uniform diffusive slab, for which all methods except SC perform well. SC overestimates the diffusion coefficent on thick cells, resulting in the observed flattening of the flux [3]. Figure 2 shows results for a test problem from [11]. In this problem, the DD cell-edge fluxes oscillate wildly about the cell-center values, cancelling in the source region on the left but leaving an error on the cell-center fluxes on the right. In both these problems, ES and LD are about equally accurate.

2.3 Slope Limiter

However, there exist unresolved boundary layer problems in which the ES method can perform poorly. The slope term given in Eq. (13) is accurate in diffusive regions or on small meshes. It is also robust in non-diffusive regions, except at material interfaces where the scattering ratio c changes and the boundary layer in the more diffusive region is not resolved by the spatial grid. The test problem from [11] displayed in Figure 3 is an example. Here, an external flux from the left strikes an absorbing region followed by a thick diffusive region with no inhomogeneous source. The boundary layer on the left edge of the diffusive region is left unresolved by our mesh. The slope estimate in Eq. (13) grossly overestimates the scattering source slope, resulting in the dramatic overshoot seen in Figure 4 without a slope limiter.

If the spatial grid resolves the boundary layer, we obtain the correct result. However, it is preferable to be as accurate as possible in cases where the solution is not adequately resolved by the grid. The robustness of

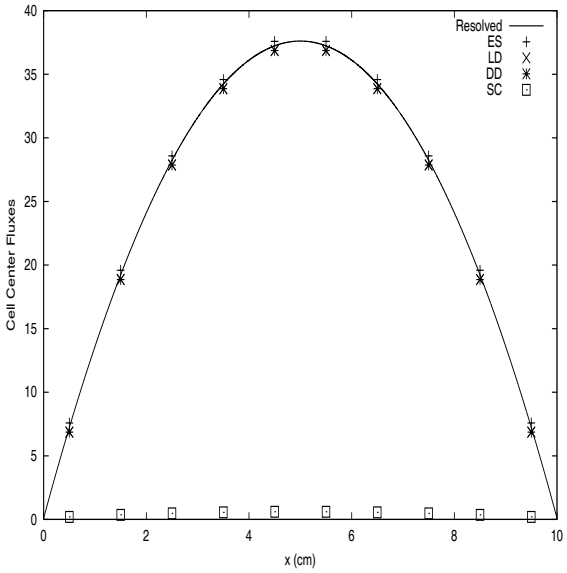

Figure 1. Uniform Diffusive Slab. Vacuum Boundaries. $Q(x) \equiv .01$. $\Sigma_t \equiv \Sigma_s \equiv 100$. $h \equiv 1$. S_{16} Gauss-Legendre quadrature. LD and DD are nearly coincident.

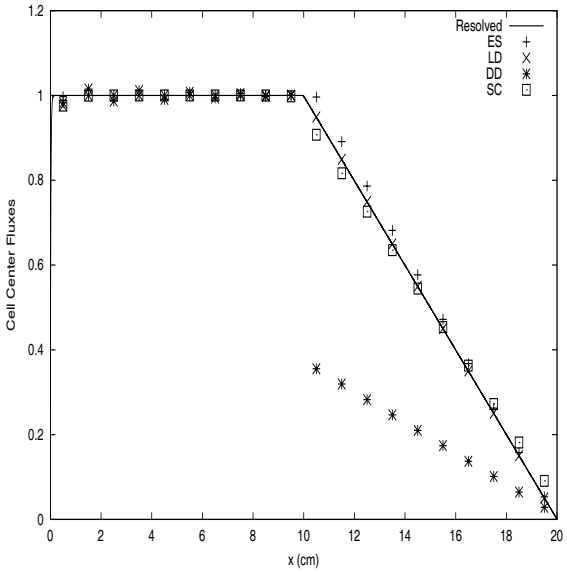

Figure 2. Vacuum boundaries. $Q(x) = 10.0$ on $0 < x < 10$ and $Q(x) = 0$ on $10 < x < 20$. $\Sigma_t \equiv 100$. $\Sigma_s = 90$ on $0 < x < 10$ and $\Sigma_s = 100$ on $10 < x < 20$. $h \equiv 1$. S_{16} Gauss-Legendre quadrature.

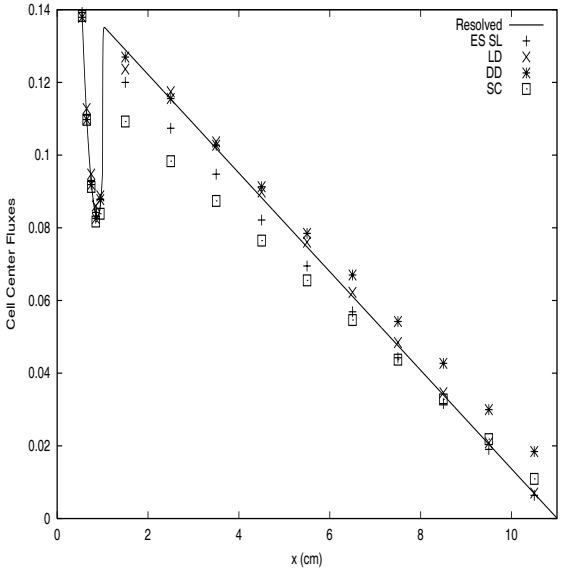

Figure 3. Left boundary incident flux $\psi(0, \mu) = 1$ for $\mu > 0$. $Q(x) \equiv 0$. $\Sigma_t = 2$ on $0 < x < 1$ and $\Sigma_t = 100$ on $1 < x < 11$. $\Sigma_s = 0$ on $0 < x < 1$ and $\Sigma_s = 100$ on $1 < x < 11$. $h = 0.1$ on $0 < x < 1$ and $h = 1$ on $1 < x < 11$. S_{16} Gauss-Legendre quadrature.

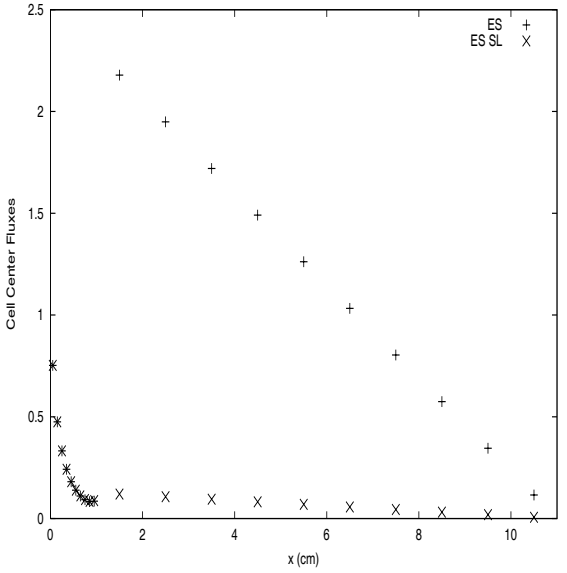

Figure 4. Same as Figure 3 (note the change in scale). Original ES is compared to slope limited ES SL.

the original slope term only degrades significantly at material (c) interfaces. Since the diffusion limit does not apply when c changes by more than $O(\epsilon^2)$, the simplest approach is to set $\hat{\phi}_{nj}$ to zero across interfaces where c changes significantly, which it does at every material interface in the test problems in Figures 1 through 5. We are investigating more sophisticated slope limiters, but this simple form suffices to illustrate the basic function. In Figures 3 and 4, we demonstrate this and call the slope limited version ES SL. ES SL reduces to ES in the thick diffusion limit and preserves linear solutions to the transport equation. ES SL is a *linear* slope limiter, since it only depends on the material properties and not on the flux values. In Figure 3 and similar problems, ES SL significantly improves accuracy without resolving the boundary layer. Employing ES SL does not appreciably change the results shown in Figures 1 and 2, or in other problems except ones with unresolved boundary layers at interfaces where c changes, as in Figure 3. Also, changing between ES and ES SL does not significantly affect any of the Krylov iterative analysis that follows, even in the random material test cases described below.

We have shown that either a linear or a characteristic approach can be used to discretize the left side of the transport equation and still meet the thick diffusion limit if the right side is discretized by the ES or ES SL method. This gives a total of four variations on the ES approach. To characterize the difference between the characteristic and linear α_{nj} terms, Eqs. (11) and (12), we simply state that the characteristic approach generally yields results closer to step characteristic (except that ES is more accurate in the diffusion limit) and that the linear approach yields results that are closer to LD. As an example, in Figure 5, we show

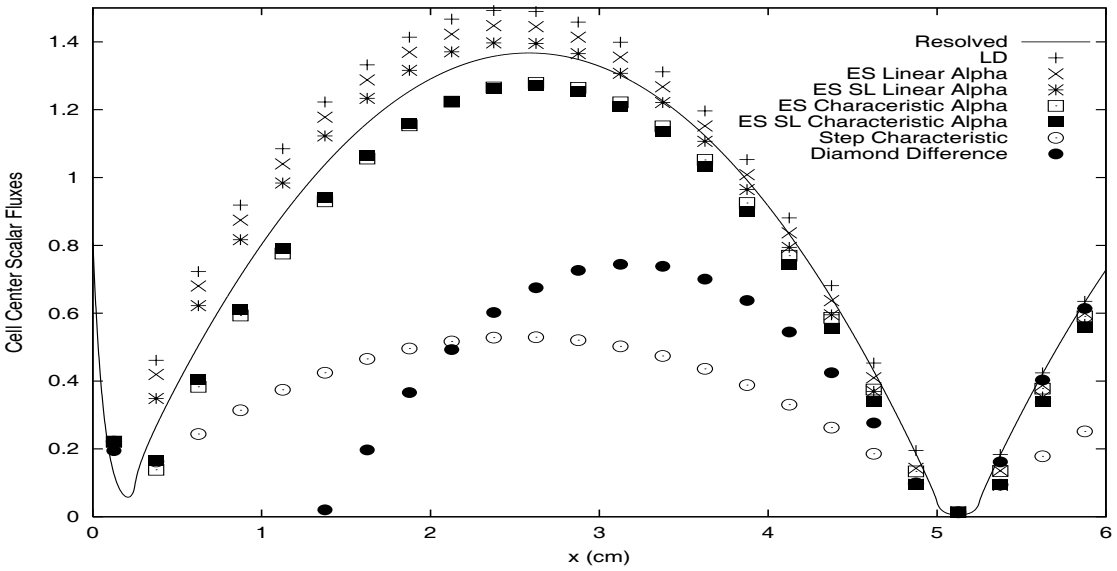

Figure 5. Left incident flux $\psi(0, \mu_n) = 30\delta_{n,1}$. $Q \equiv 0.01$. $\Sigma_t \equiv 15$. $\Sigma_s = 15$ on $0.25 < x < 5.0$ and $5.25 < x < 10$ $\Sigma_s = 0$, otherwise. $h \equiv 0.25$. S_{16} Gauss-Legendre quadrature.

results from a problem with a highly anisotropic flux incident on the left boundary of a slab. The first cell and the cell from $x = 5$ to $x = 5.25$ are pure absorbers, the rest are purely diffusive, and all cells are 3.75 mean free paths thick. SC and DD both fail for this problem, and even LD overestimates the flux due to the unresolved boundary layer. Characteristic ES and ES SL both underestimate the flux slightly and are not too different from each other. Linear ES and ES SL both fall between the exact solution and the LD solution. Linear ES SL with the slope limiter is more accurate here than linear ES. More generally, ES SL is more accurate than SC and DD but less accurate than LD, and use of the characteristic versus the linear left side discretization shifts the solution a little more toward the LD or the SC solution without

significantly affecting accuracy.

We have considered other slope limiters, both linear like ES SL and nonlinear (dependent on the fluxes, which is undesirable). A linear slope limiter can also be regarded as part of the definition of the slope term, augmenting Eq. (13). ES SL was presented to illustrate the intended slope limiter function. We are actively investigating slope limiters and/or improvements to the slope term definition, such as ES SL, that do not change the diffusion limit properties of the method, but that are improvements over ES SL.

3. ADDITIVE DSA ITERATIVE ANALYSIS

The consistent (four-step) DSA approach [5] for ES yields a complicated symmetric indefinite 5-point stencil for the cell-center scalar fluxes in 1-D. On the other hand, the leading order discrete asymptotic equation is a standard, symmetric-positive-definite, 3-point, cell-centered diffusion stencil. Because use of modified asymptotic diffusion equations for acceleration has worked for LD methods [5, 12], we consider use of the asymptotic cell-centered diffusion equation for inconsistent DSA (IDSA).

We assume an infinite grid of period J in which all quantities except position on cell j are the same on cell $j+J$. The homogeneous balance and auxiliary equations for each direction, $n = 1:N$, and cell, $j = 1:J$, become

$$-\frac{\mu_n}{t_j}\psi_{n,j-\frac{1}{2}} + \frac{\mu_n}{t_j}\psi_{n,j+\frac{1}{2}} + \psi_{n,j} = \frac{c_j}{2}\phi_j \tag{20}$$

$$\begin{aligned} -\frac{1-\alpha_{nj}}{2}\psi_{n,j-\frac{1}{2}} - \frac{1+\alpha_{nj}}{2}\psi_{n,j+\frac{1}{2}} + \psi_{n,j} &= \left[\frac{\alpha_{nj}c_j}{4}\frac{t_j}{t_j + t_{j+\frac{\mu_n}{|\mu_n|}}}\left(1-\frac{\mu_n}{|\mu_n|}\right)\right]\phi_{j-1} \\ &+ \left\{\begin{array}{l} \left[\frac{\alpha_{nj}c_j}{4}\frac{t_j}{t_j+t_{j+\frac{\mu_n}{|\mu_n|}}}\left(1+\frac{\mu_n}{|\mu_n|}\right)\right] \\ -\left[\frac{\alpha_{nj}c_j}{4}\frac{t_j}{t_j+t_{j+\frac{\mu_n}{|\mu_n|}}}\left(1-\frac{\mu_n}{|\mu_n|}\right)\right] \end{array}\right\}\phi_j \\ &- \left[\frac{\alpha_{nj}c_j}{4}\frac{t_j}{t_j + t_{j+\frac{\mu_n}{|\mu_n|}}}\left(1+\frac{\mu_n}{|\mu_n|}\right)\right]\phi_{j+1}, \end{aligned} \tag{21}$$

where c_j is the scattering ratio in cell j and closure is achieved by setting $\psi_{n,j(\pm\frac{1}{2})} = \psi_{n,j+J(\pm\frac{1}{2})}$ for all n and $\phi_{j+J} = \phi_j$. We change variables to the Fourier error mode,

$$\phi_j^{(l)} = \phi_j e^{i\lambda x_j} \tag{22}$$

$$\psi_{nj}^{(l+\frac{1}{2})} = \psi_{nj} e^{i\lambda x_j} \tag{23}$$

$$\psi_{n,j\pm\frac{1}{2}}^{(l+\frac{1}{2})} = \psi_{n,j\pm\frac{1}{2}} e^{i\lambda x_{j\pm\frac{1}{2}}}, \tag{24}$$

where l is the starting iteration index and $l+\frac{1}{2}$ is the index after a source iteration sweep. For analysis, we code our system of $2NJ$ equations, (20) and (21), directly as the linear system

$$L\psi^{(l+\frac{1}{2})} = M\phi^{(l)}, \tag{25}$$

and simplify to the J vector update

$$\phi^{(l+\frac{1}{2})} = PL^{-1}M\phi^{(l)} = X_{SI}\phi^{(l)}, \tag{26}$$

where P integrates the cell center angular errors to a scalar error. X_{SI} is the source iteration operator; its largest eigenvalue is the spectral radius of the transport part of each iteration. We solve for the approximate scalar error correction, $F \approx \phi - \phi^{(l+\frac{1}{2})}$, using the cell-centered diffusion equation [Eq. (19)], coded for analysis as the linear system

$$DF = S\left(\phi^{(l+\frac{1}{2})} - \phi^{(l)}\right), \tag{27}$$

where $S = diag(\Sigma_{sj} h_j)$ represents multiplication by the scattering cross section. We find that the corrected scalar error vector is

$$\begin{aligned} \phi^{(l+1)} &= F + \phi^{(l+\frac{1}{2})} \\ &= D^{-1}S\left(X_{SI}\phi_j^{(l)} - \phi_j^{(l)}\right) + X_{SI}\phi^{(l)} \\ &= \left[X_{SI} - D^{-1}S\left(I - X_{SI}\right)\right]\phi^{(l)} \qquad (28) \\ &= X_{IDSA}\phi^{(l)}. \qquad (29) \end{aligned}$$

Here, X_{IDSA} is the IDSA iteration operator based on Eq. (19), and the largest eigenvalue of X_{IDSA} is the spectral radius for the period-J grid and material properties considered. In the case of an infinite homogeneous medium and grid, X_{SI} and X_{IDSA} are one-dimensional, and X_{IDSA} as a function of cell optical thickness is plotted in Figure 6. Nearly all of the heterogeneous features of IDSA can be analyzed

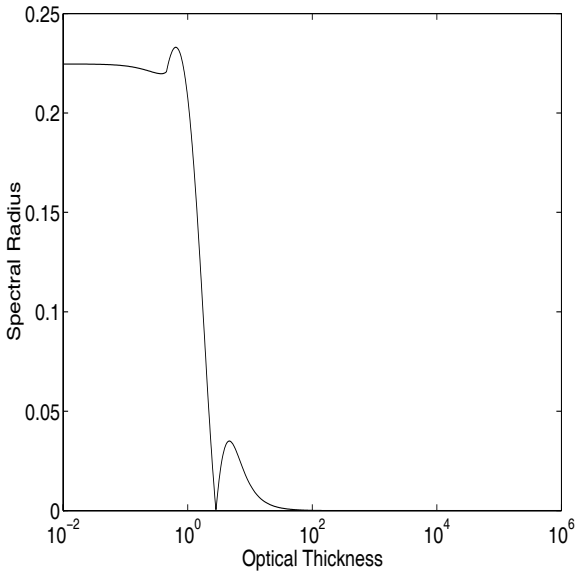

Figure 6. Homogeneous case.

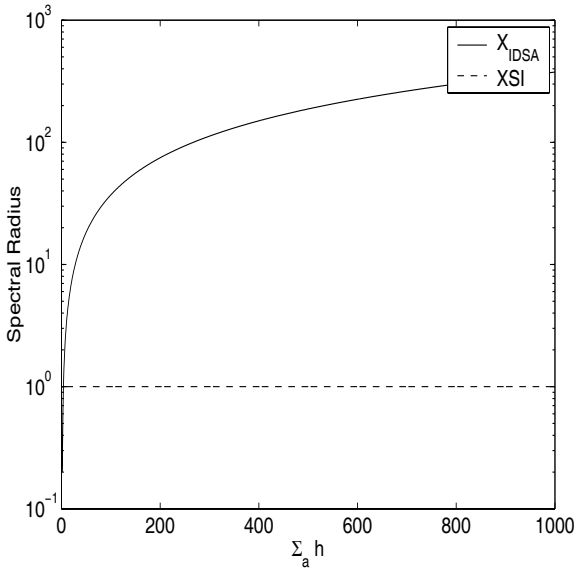

Figure 7. SI and accelerated spectral radius for values of $\Sigma_t h = \Sigma_a h$ in the first two cells and $\Sigma_s h = \Sigma_t h = 100$ in the latter two cells.

by setting $J = 4$, with generally different values of optical thickness, τ_j, and scattering ratio, c_j, in each of the 4 cells, $j = 1 : 4$, but repeating in an infinite medium. Making the first two cells absorbers and the last two cells diffusive, we see one of the worst-case instabilities in Figure 7, where the spectral radius grows linearly in $\Sigma_a h$ in the first two cells. Hence, IDSA for the ES scheme is stable for uniform media and grids (Figure 6), but is unstable in heterogeneous media with optically thick cells. We have verified these Fourier analysis predictions in a Fortran test code which has subroutines to perform ES source iteration and to invert the cell-centered diffusion operator for IDSA.

We have derived and examined several other DSA schemes for the explict slope method. None have ideal characteristics. In particular, if we use the four-step approach [5], we obtain a non-standard, symmetric indefinite, discretization of the diffusion equation which has a 5-point stencil in 1-D. Fourier analysis of the four-step DSA scheme for hard heterogeneous cases like Figure 7 reveals ideal performance similar to that of the cell-centered method in the homogeneous case. However, the expense of solving the larger stencil and the complexity of its derivation (particularly if we consider extension to multiple dimensions) seems to rule out practical use of consistent DSA with the ES method.

4. KRYLOV SOLUTION METHODS

We consider the discretized ES S_N equations (using the same notation as in the Fourier analysis section, but without implying complex exponentials or periodicity),

$$L\psi = M\phi + q.$$

Inverting the left hand side and integrating over all directions, we obtain

$$\begin{aligned} \phi &= PL^{-1}M\phi + PL^{-1}q \\ &= X_{SI}\phi + \phi_{unc}, \end{aligned} \tag{30}$$

or

$$(I - X_{SI})\phi = \phi_{unc}. \tag{31}$$

where ϕ_{unc} is the uncollided scalar flux due to inhomogeneous internal and boundary sources. We can easily solve the linear system, Eq. (31), using any standard non-symmetric transpose-free Krylov solver [6, 8], such as GMRES or BICGSTAB, with reverse communication that calls on our source iteration routine to perform the action of X_{SI}. Specifically, we first calculate ϕ_{unc} by calling our source iteration routine with normal inhomogeneous boundary conditions and internal sources. The system in Eq. (31) then has homogeneous boundary conditions, and calls to the source iteration routine are made accordingly, with homogeneous boundary conditions and no internal sources. This reflects that the collided flux, ϕ in Eq. (31), physically has no inhomogeneous boundary or internal sources. We handle reflective boundary conditions, including opposing reflective boundary conditions, in the same implicit fashion as [8], augmenting the scalar flux vector with boundary angular fluxes. If the diffusion operator considered in the DSA analysis exactly corrected the iteration error, then X_{IDSA} would vanish and it is clear from Eq. (28) that

$$(I - X_{SI})(I + D^{-1}S) = I. \tag{32}$$

It is thus natural to use the operator

$$M^{-1} = (I + D^{-1}S) \tag{33}$$

as a preconditioner, with reverse communication demanding a subroutine to solve the cell-centered diffusion system

$$D\phi = Sr \tag{34}$$

for any right hand side r. Of course, we simply use the same IDSA subroutine as in our regular (simple iteration) Fortran test code that inverts the cell-centered diffusion operator.

We now make an intuitive argument that the asymptotic cell-centered discretization of the diffusion equation is appropriate and effective for solution of Eq. (31) by GMRES. The cell-centered diffusion operator is symmetric positive definite, implying that $(I + D^{-1}S)$ is also symmetric positive definite. For

non-supercritical systems, the eigenvalues of $(I - X_{SI})$ are bounded in magnitude between 0 and 1 in the positive real half-plane. Heuristically, the effect of preconditioning will be to shift the spectrum of the operator away from the origin. In particular, the smallest eigenvalues of $(I - X_{SI})$, corresponding to diffusive modes, are moved from close to the origin to close to unity by the preconditioner as per Eq. (32). We have analyzed this spectral effect for periodic problems with similar analysis machinery as was used in the Fourier analysis of IDSA. Generally, IDSA is unstable for problems with optically thick heterogeneities, but cell-centered diffusion preconditioned Krylov is still extremely effective. In many problems where IDSA is unstable, like the random material test cases described below, the preconditioner shifts the eigenvalues to a compact cluster about unity, meaning that the preconditioner is very effective. However, in certain cases of *hard periodic* heterogeneities, the preconditioner shifts the corresponding eigenvalues to multiple clusters, away from both unity and the origin. Each cluster corresponds to a type of periodic heterogeneity in the problem (of which there can only be a small number relative to the system dimension). Our numerical results, as well as intuition, suggest that this poses little difficulty for the Krylov method. The reason for this is roughly as follows [6, 7]. The preconditioned GMRES method at step l minimizes the 2-norm of the residual over the Krylov space spanned by the operator polynomial of degree l that takes value 1 at the origin, in the right or left preconditioned operator $A = (I - X_{SI})M^{-1}$ or $A = M^{-1}(I - X_{SI})$,

$$||r^{(l)}|| = \min_{p_l(0)=1} ||p_l(A)r^{(0)}||. \tag{35}$$

If A is not normal, one cannot evaluate Eq. (35) purely in terms of the spectrum or condition number of A. However, if we assume A is diagonalizable, $A = S^{-1}DS$ with $D = diag(eig(A))$, then Eq. (35) becomes

$$||r^{(l)}|| \leq \text{cond}\,(S) \min_{p_l(0)=1} ||p_l(D)r^{(0)}||, \tag{36}$$

and we can write the polynomial in D as a polynomial in the eigenvalues of A. If A is normal, then cond(S)=1, but since A is non-normal for the ES and many other S_N discretization schemes, we have that cond(S)≥ 1. Neglecting the non-normality, we see that the minimum polynomial of eigenvalues of A is achieved in the least number of iterations when A's eigenvalues are tightly clustered away from the origin, because the polynomial $(1 - z/c)^l$ is small if all its roots are close to some scalar c. Thus, GMRES should perform better as the preconditioned eigenvalues become tightly clustered about points away from the origin in the complex plane. Though this argument does not hold strictly for non-normal operators, it does provide a heuristic guide and is in agreement with our numerical testing, at least in 1-D.

The four-step operator is potentially a better preconditioner than the cell-centered diffusion operator. It can yield tighter cluster of eigenvalues about unity, instead of creating additional clusters corresponding to hard periodic heterogeneous modes. However, due to the four-step operator's complexity and large stencil, we do not consider this to be a practical approach. After extensive testing (described below) of diffusive problems, problems with hard periodic heterogeneities, and random material problems, we conclude that in 1-D the asymptotic cell-centered diffusion preconditioner is never significantly deleterious. Furthermore, in all cases where the unpreconditioned Krylov iteration is slow due to diffusive eigenmodes, the cell-centered preconditioner is extremely effective. In other cases, where the unpreconditioned Krylov method is effective by itself, application of the cell-centered preconditioner has no significant effect on convergence, even in cases where IDSA is grossly unstable due to hard periodic heterogeneities.

In Table I, we compare and analyze the computational cost of unpreconditioned Krylov, cell-centered diffusion-preconditioned Krylov, source iteration (SI), and additive IDSA by iteration counts. We only present results for the restarted GMRES method with right-preconditioning, but limited testing of left-preconditioning and BICGSTAB indicates similar trends for these approaches. We intend to investigate other Krylov methods more thoroughly in the future.

Table I. Krylov Iteration Counts, 10,000 cell 1-D Test Problems.

Problem τ	Unpreconditioned GMRES(20)	Diffusion Preconditioned GMRES(20)	SI	IDSA
Homogeneous Medium ($c = .9999$) of Cell Thickness τ:				
1	1953	6	$184,200^{\dagger}$	12
10	105	3	$184,200^{\dagger}$	5
100	10	2	$184,200^{\dagger}$	4
1000	3	2	$184,200^{\dagger}$	3
Random τ and c, $\tau = \max_j \tau_j$, $0 < c_j < 1$				
1	23	8	114	12
10	69	26	†	$\star$
100	288	56	†	$\star$
1000	1394	19	†	$\star$
Random τ and c, $\tau = \max_j \tau_j$, $0 < c_j < .9$				
1	17	7	58	11
10	25	18	94	150
100	29	17	122	$\star$
1000	31	14	127	$\star$
Random τ and c, $\tau = \max_j \tau_j$, $.9 < c_j < 1$				
1	51	8	513	14
10	129	23	†	76
100	475	47	†	$\star$
1000	1177	19	†	$\star$
Period-4 $\Sigma_t h = [\tau; \tau; 100; 100]$, $c = 0.9999\,[0; 0; 1; 1]$				
1	8	4	$106,980^{\dagger}$	16
10	6	5	$50,572^{\dagger}$	$\star 1.2$
100	6	4	$13,418^{\dagger}$	$\star 9.3$
1000	6	4	$7,723^{\dagger}$	$\star 21.5$

† Failed to converge in 2000 iterations or estimated from spectral radius.
$\star$ Unstable, Spectral Radius is displayed for non-random cases.

For both IDSA and for preconditioning the Krylov solver, we use the asymptotic cell-centered diffusion discretization. We show results for three classes of problems: homogeneous-medium diffusive problems, random material problems, and periodic-medium problems in which IDSA is unstable. In all problems we use 10,000 spatial cells to give non-trivial work to the solver. Each problem has vacuum boundaries and a uniform $Q = 0.01$ inhomogeneous source. For each class of problems, a characteristic optical thickness, τ, is indexed in the left hand column. In diffusive problems, τ is the thickness of each cell; in random material problems, τ is the maximum allowed cell thickness; and in periodic-medium problems, the variation of properties over a period of four cells is indicated in the table. In the random cases, for each value of τ, we assign random optical thicknesses to each of the 10,000 cells with a uniform distribution between 10^{-6} and τ. We then assign a random scattering ratio, c, to each cell with the uniform distribution indicated in the table. We terminated all problems at 10^{-8} tolerance or 2000 iterations, and in stable cases where we can calculate the spectral radius from Fourier analysis, we list the estimated number of iterations to converge. Comparison of the actual number of iterations to spectral radius-based estimates agreed to within $\pm 15\%$ for problems that converged within 2000 iterations. The 10^{-8} tolerance was applied consistently to the 2-norm of the actual residual in all calculations, $r = \phi_{unc} - (I - X_{SI})\phi^{(k)}$.

In the homogeneous-medium diffusive problems grouped at the top of Table I, we see both expected results and results that are unusual, but that we attempt to explain. Source iteration, of course, performs very poorly for such problems, with a spectral radius of $c = 0.9999$. IDSA is very effective, as expected, since there are no heterogeneities. What is unexpected is that the unpreconditioned Krylov method is increasingly effective as τ increases. We can explain this by examining the distribution of eigenvalues of $I - X_{SI}$ in the complex plane using our analysis machinery for an infinite periodic grid of small period J (an approximation of the 10,000 cell grid). For optically thin problems, the eigenvalues of $I - X_{SI}$ are distributed along the real axis between $1 - c$ and 1. As τ increases, the eigenvalues all migrate to $1 - c$. In Figures 8 and 9, for example, we show the eigenvalue distributions of the unpreconditioned and preconditioned operators of a similar period-J (J=80) problem for $\tau = 1$ and $\tau = 100$. In these problems, each cell effectively sees some leakage into the cells around it, and that leakage decreases as the optical thickness of the cell increases. The grid induces a spread in the distribution of eigenvalues of X_{SI} for optically thin meshes, even though the material is uniform. As τ increases, the eigenvalues of $I - X_{SI}$ all migrate toward $1 - c$ and are more tightly clustered, at a finite distance from the origin (since the problem is subcritical). This clustering results in the performance gains shown in Table 1 for unpreconditioned GMRES as τ increases. Even though this is a discretized homogeneous problem, and homogeneous Fourier analysis predicts the spectral radius of X_{SI} in terms of a single parameter c, a heterogeneous analysis is required to say anything about the distribution of eigenvalues induced by the grid. By doing this analysis on a period-J grid, we are able to at least qualitatively understand the behavior of the Krylov method. We note that in all of the homogeneous-media cases, the preconditioned Krylov method performed very well. Analysis of the preconditioned eigenvalue distribution shows that the diffusion precondtioner, in these cases, simply moves all of the eigenvalues to a tight cluster about unity, tighter as τ increases (see Figures 8 and 9), resulting in optimal performance of the Krylov solver. This is because Eq. (32) is nearly exact, and the preconditioned operator is a close approximate identity.

The purpose of the random material calculations is to measure the effectiveness of the cell-centered preconditioner when the eigenvalue distribution is non-clustered. The eigenvalues of X_{SI} are clustered in the optically thick diffusive cases above and in the periodic cases below. The random material and scattering ratio assignments described above result in a random distribution of eigenvalues of X_{SI}. As can be seen in the table, as the maximum optical thickness increases, the unpreconditioned Krylov method, as well as source iteration, take longer to converge. This is because, analogous to the homogeneous cases above, the diffusive eigenvalues of $I - X_{SI}$ migrate toward their values of $1 - c_j$ as τ_j increases (j

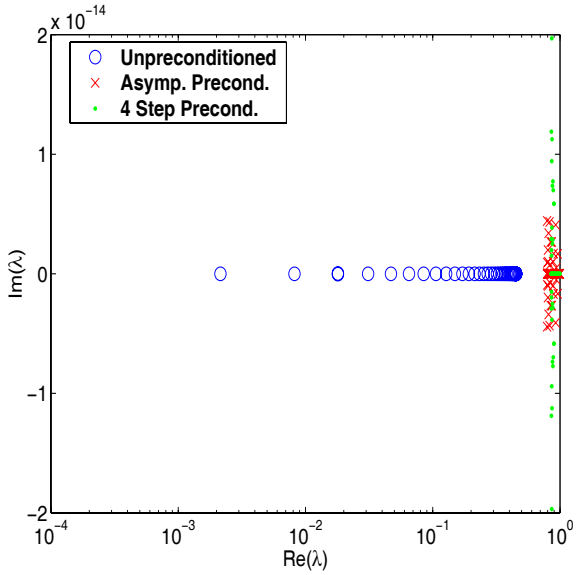

Figure 8. Homogeneous-Medium (as in Table 1) preconditioned operator eigenvalue distributions. $\tau = 1$. J=80 cells. Periodic BC's. S_8 Gauss-Legendre quadrature.

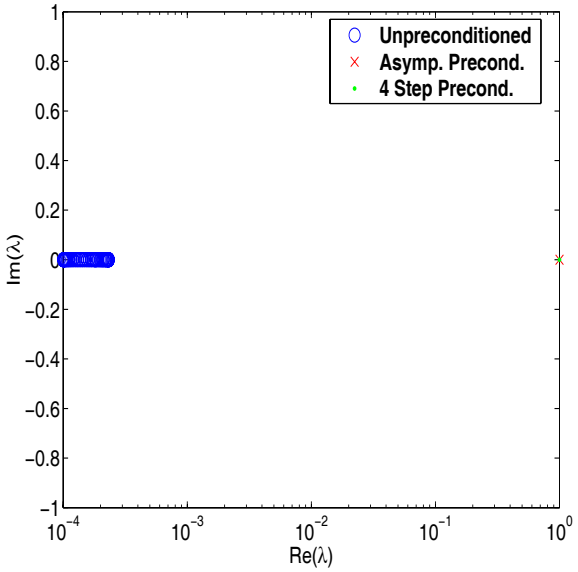

Figure 9. Homogeneous-Medium (as in Table 1) preconditioned operator eigenvalue distributions. $\tau = 100$. J=80 cells. Periodic BC's. S_8 Gauss-Legendre quadrature. Both preconditioned operators are approximate identities.

corresponds to a cell, $j = 1, ..., 10,000$). Unlike the homogeneous cases above, the value of $1 - c_j$ is randomly assigned in every cell, so no clustering occurs. In Figures 10 and 11, for example, we show the period-J eigenvalue distributions for $\tau = 1$ and $\tau = 100$. In the absence of favorable clustering, like that seen in the homogeneous case above, the Krylov performance degrades as eigenvalues get closer to zero. If we partition the allowed values of c to be either less than or greater than 0.9, we can see this more clearly, as shown in Table I. For $0 < c < 0.9$, even though no special clustering occurs, unpreconditioned Krylov is effective because there are no eigenvalues close to zero. For $0.9 < c < 1$, the unpreconditioned Krylov performance deteriorates as the unclustered diffusive eigenvalues migrate toward $1 - c_j$ (which is close to zero in many cells – the problem is getting closer to criticality). This explains the observed performance deterioration of the unpreconditioned Krylov solver. Yet, the cell-centered diffusion preconditioned Krylov solver remains very effective, even in cases where IDSA is unstable. This is because the preconditioner exactly counteracts the effect of the diffusive eigenvalues by moving them from near the origin to near unity, again in accordance with Eq. (32). The preconditioner acts as well to cluster the non-diffusive eigenvalues, though not in all cases as close to unity as would a consistent diffusion preconditioner such as is generated by the four-step method. In fact, investigating the eigenvalue distributions of period-J meshes with random grid and material properties, as in Figures 10 and 11, we see that the preconditioner acts to cluster nearly all of the eigenvalues close to unity. As seen in Table I, this is slightly less effective for intermediate optical thicknesses. Eigenvalue analysis of the four-step preconditioner on period-J meshes shows that it would not see this dip in performance, because it achieves a tighter cluster of the eigenvalues about unity, as in Figure 11.

The periodic media calculations grouped last in Table I assess the performance of the cell-centered preconditioner in cases where IDSA is unstable due to hard periodic heterogeneities, just like in Figure 7. As can be seen in Table I, the unpreconditioned Krylov method is very fast for these problems because of

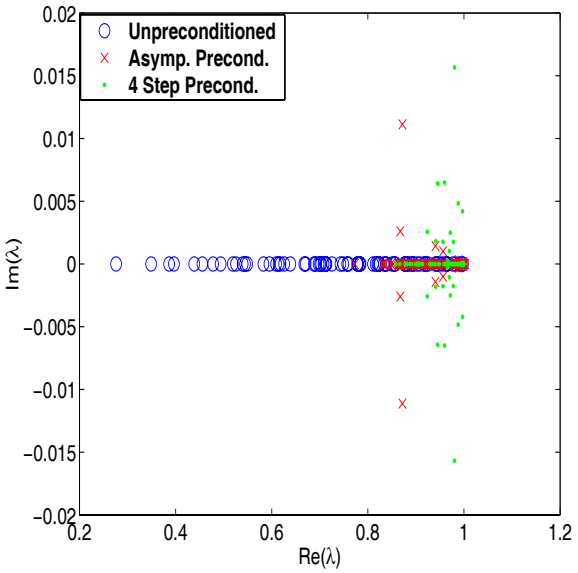

Figure 10. Random Material ($0 < c < 1$, as in Table 1) preconditioned operator eigenvalue distributions. $\tau = 1$. J=80 cells. Periodic BC's. S_8 Gauss-Legendre quadrature.

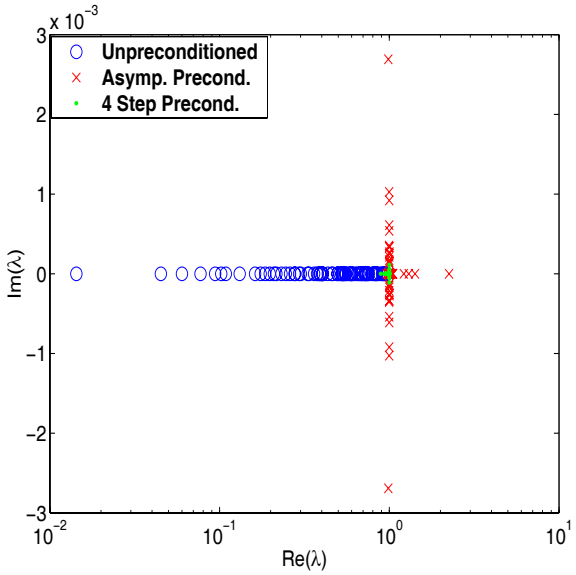

Figure 11. Random Material ($0 < c < 1$, as in Table 1) preconditioned operator eigenvalue distributions. $\tau = 100$. J=80 cells. Periodic BC's. S_8 Gauss-Legendre quadrature.

the tight clustering of eigenvalues induced by optically thick periodicity, displayed for example in Figures 12 and 13. The preconditioner has little effect on performance. Yet, it is only for these types of problems (hard periodic heterogeneities) that the cell-centered preconditioner can sometimes cost more iterations than the unpreconditioned case. However, the cost is trivial (only a few iterations) in every case we have observed. This is because the preconditioner clusters the eigenvalues corresponding to hard periodic heterogeneities, of which there can only be a small number relative to the system dimension. Since isolated clusters of this type are handled very effectively by the Krylov method, they do not cause significant problems; at the most, they cost a few extra iterations. For these cases, the preconditioned Krylov method is nearly equivalent to the unpreconditioned Krylov method, as seen in Table I.

6. DISCUSSION

In conclusion, we have developed a new ES spatial discretization scheme for S_N equations. This method preserves the linear transport solutions, requires only one unknown per cell, and satisfies the asymptotic diffusion limit. From an accuracy viewpoint, the ES method is a significant advance over previous S_N discretizations schemes that contain only one fundamental unknown per spatial cell. With the linear approach [Eq. (12)] to discretizing the left side and the addition of an effective slope limiter, ES is computationally efficient and approaches the accuracy of LD, but without the additional unknown per cell. ES is also simpler to precondition, using the cell-centered diffusion discretization either in IDSA for optically thin problems or as a Krylov preconditioner for general problems.

Our method of analyzing Krylov performance is not rigorous, but is very useful. Transport operators are non-normal, and their behavior may not be governed simply by their eigenmodes. However, our approach does seem to explain the performance trends we have observed for the ES method. The calculation of transport operator eigenvalue distributions (both unpreconditioned and preconditioned) for a large problem

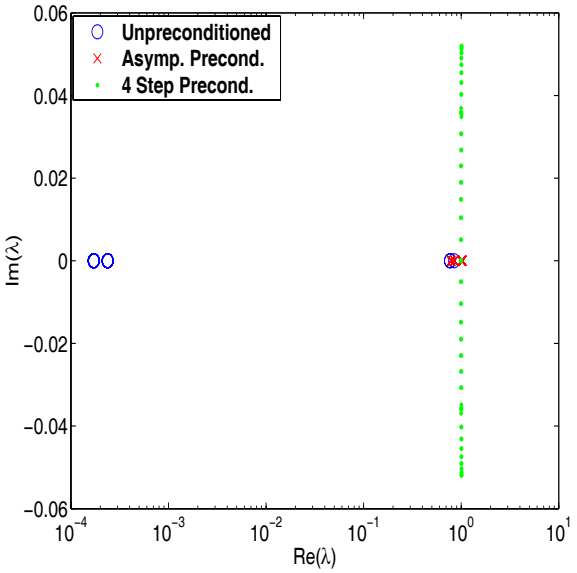

Figure 12. Periodic Absorber-Diffuser (as in Table 1) preconditioned operator eigenvalue distributions. $\tau = 1$. J=80 cells. Periodic BC's. S_8 Gauss-Legendre quadrature.

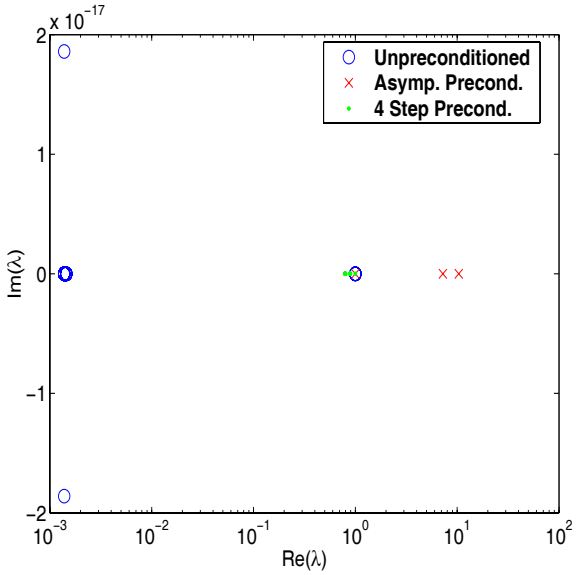

Figure 13. Periodic Absorber-Diffuser (as in Table 1) preconditioned operator eigenvalue distributions. $\tau = 100$. J=80 cells. Periodic BC's. S_8 Gauss-Legendre quadrature.

is a computationally demanding task. Calculating the eigenvalues of a similar, smaller, heterogeneous problem with periodic boundary conditions is easily accomplished, as is heterogeneous Fourier analysis. We see a direct relationship between the eigenvalue distributions we have calculated and the performance of the Krylov method on similar problems that are much larger and non-periodic.

Though we did not implement the four-step preconditioner in our Fortran test code, we did investigate it via numerical analysis. In particular, we analyzed the preconditioned eigenvalue distributions for period-J versions of all the problems in Table I. Comparing the four-step preconditioner to the asymptotic cell-centered preconditioner, as in Figures 8 through 13, we observe that both act to cluster nearly all of the preconditioned eigenvalues near to unity. In many cases, one preconditioner does a slightly better job of this than the other, but only in the cases of hard periodic heterogeneities does the cell-centered preconditioner do anything unusual. The cell-centered preconditioner always moves diffusive eigenvalues from close to the origin to close to unity. However, in these periodic heterogeneity cases, the cell-centered preconditioner tends to cluster the corresponding eigenvalues away from unity, much as the unpreconditioned operator does, but frequently with tighter clusters. In these cases, the four-step preconditioner may perform better than the cell-centered preconditioner. However, because of the complexity and indefiniteness of the four-step operator, and because use of the cell-centered operator has not been more than trivially detrimental in any case investigated to date, we believe that the cell-centered preconditioner, despite the fact that it can cause IDSA to become unstable, is a robust Krylov preconditioner for general problems with the 1-D ES method.

We are continuing to research all aspects of the ES discretization scheme, including better employment of slope limiters, Krylov performance, and extension to multi-dimensional problems.

ACKNOWLEDGEMENTS

This work was supported by the DOE Computational Science Graduate Fellowship program, and was started during a student practicum supervised by Jim Morel at Los Alamos National Laboratory. We gratefully acknowledge several helpful suggestions by Jim Morel and James Warsa of Los Alamos National Laboratory.

REFERENCES

[1] H.L. Hanshaw and E.W. Larsen, "An Explicit Slope S_N Differencing Scheme," *Trans. Am Nucl Soc* **87**, (November, 2002).

[2] R.E. Alcouffe, E.W. Larsen, W.F. Miller, Jr. and B.R. Wienke, "Computational Efficiency of Numerical Methods for the Multigroup, Discrete-Ordinates Neutron Transport Equations: The Slab Geometry Case," *Nucl. Sci. Eng.* **71**, 111 (1979).

[3] E.W. Larsen, "Infinite Medium Solutions of the Transport Equation, S_N Discretization Schemes, and the Diffusion Approximation," *Proceedings, ANS International Meeting on Mathematical Methods for Nuclear Applications,* Salt Lake City, USA, 2001.

[4] E.W. Larsen, J.E. Morel, and W.F. Miller, Jr., "Asymptotic Solutions of Numerical Transport Problems in Optically Thick, Diffusive Regimes," *J. Comp. Phys.* **69**, 2 (1987).

[5] M.L. Adams and E.W. Larsen, "Fast Iterative Methods for Discrete-Ordinates Particle Transport Calculations," *Prog. Nucl. Energy* **40**, 3 (2002).

[6] Y. Saad, *Iterative Methods for Sparse Linear Systems*, PWS Publishing Company: Boston (1996).

[7] A. Greenbaum, *Iterative Methods for Solving Linear Systems,* SIAM (1997).

[8] J.S. Warsa, T.A. Wareing, and J.E. Morel, "Diffusion Synthetic Acceleration - Part II: Krylov Methods for Multi-Dimensional Heterogeneous Problems," submitted to *Nuclear Science and Engineering* in 2001.

[9] E W. Larsen. "Unconditionally Stable Diffusion-Synthetic Acceleration Methods for the Slab Geometry Discrete Ordinates Equations. Part 1: Theory," *Nuclear Science and Engineering.* **82**, 47 (1982).

[10] J.E. Morel and E. W. Larsen, "A Multiple Balance Approach for Differencing the S_N Equations," *Nuclear Science and Engineering.* **105**, 1-15 (1990).

[11] E.W. Larsen and J.E. Morel, "Asymptotic Solutions of Numerical Transport Problems in Optically Thick, Diffusive Regimes II," *J. Comp. Phys.* **83**, 1 (1989).

[12] T. Wareing, *Asymptotic Diffusion Accelerated Discontinuous Finite Element Methods for Transport Problems.* PhD. Thesis, University of Michigan (1991).